Brand, Jonathan; Néel, Nicolas; Kröger, Jörg:

Probing relaxations of atomic-scale junctions in the Pauli repulsion range

Original published in:	New journal of physics / Institute of Physics. - [Bad Honnef] : Dt. Physikalische Ges. - 21 (2019), October, art. 103041, 10 pp.
Original published:	2019-10-23
ISSN:	1367-2630
DOI:	10.1088/1367-2630/ab4c84
[*Visited:*	2019-12-10]

New Journal of Physics
The open access journal at the forefront of physics

Deutsche Physikalische Gesellschaft DPG IOP Institute of Physics

PAPER • OPEN ACCESS

Probing relaxations of atomic-scale junctions in the Pauli repulsion range

To cite this article: J Brand *et al* 2019 *New J. Phys.* **21** 103041

New Journal of Physics
The open access journal at the forefront of physics

Deutsche Physikalische Gesellschaft DPG
IOP Institute of Physics

Published in partnership with: Deutsche Physikalische Gesellschaft and the Institute of Physics

OPEN ACCESS

RECEIVED
19 June 2019

REVISED
17 September 2019

ACCEPTED FOR PUBLICATION
9 October 2019

PUBLISHED
23 October 2019

PAPER

Probing relaxations of atomic-scale junctions in the Pauli repulsion range

J Brand, N Néel and J Kröger

Institut für Physik, Technische Universität Ilmenau, D-98693 Ilmenau, Germany

E-mail: joerg.kroeger@tu-ilmenau.de

Keywords: atomic force microscopy, scanning tunnelling microscopy, single-molecule junction, C60, surface physics, adsorption, surface chemistry

Abstract

Clean metal as well as C_{60}-terminated tips of an atomic force microscope probe the interaction with C_{60} molecules adsorbed on Cu(111) and Pb(111). The force measurements unveil a monotonic shift of the point of maximum attraction with the bias voltage. The conventional superposition of long-range van der Waals and electrostatic forces with short-range Pauli repulsion does not reproduce the shift. By phenomenologically including bias-dependent relaxations of the electrode geometry in the analytical expression for the short-range force the experimental data can qualitatively be described.

1. Introduction

The measurement of forces between atoms and molecules that are on the verge of forming a chemical bond belongs to the fascinating capabilities of an atomic force microscope (AFM). For instance, approaching the force sensor into the Pauli repulsion distance range where the orbital overlap between the atomic probe and a molecule is significant enables imaging of the molecular skeleton [1–3]. Another example is the manipulation of matter at the atomic scale, which involves the intentional movement of single atoms and molecules across a surface using the scanning probe. The required lateral forces were previously determined in AFM experiments [4].

At and close to chemical-bond distances adhesive forces can induce relaxations of the atomic electrode geometry [5–14]. Mechanical hysteresis [15, 16] or even fracture of the electrode material [10] may be the response to these strong forces. Such atomic relaxations represent the elementary processes in friction and cause dissipation and wear [17]. It was further demonstrated that atom rearrangements in single-atom and single-molecule junctions have a profound impact on electron transport across the junction [18–20]. Indeed, the number and transmission of transport channels depend on the actual junction geometry of atomic [21] and molecular [22] contacts. Moreover, orientations and conformations of adsorbed molecules matter in the conductance of the ballistic transport junction [23–25], induce multilevel conductance variations [26, 27] and changes in Andreev reflection for normal-metal–superconductor contacts [28]. The controlled atom-by-atom modification of electrodes was demonstrated to yield order-of-magnitude changes in the junction conductance [29, 30]. Magnetoresistive [31–37] and spin valve [38, 39] effects were likewise reported to be influenced by the actual relaxed junction geometry.

Consequently, ample interest is directed towards atomic relaxations in junctions with ultimate dimensions and towards the underlying forces. Here, a combination of scanning tunnelling microscope (STM) and AFM experiments are presented that unravel an unexpected shift of the point of maximum attraction between two C_{60} molecules with the bias voltage applied across the molecular junction. The prototypical junctions investigated consist of a C_{60}-terminated metal tip and a C_{60} molecule adsorbed on Cu(111). A similar shift is present for a clean metal tip and C_{60} adsorbed on Pb(111). The superposition of long-range van der Waals and electrostatic attraction with short-range Pauli repulsion does not reproduce the monotonic variation of the contact point. A qualitative description of the experimental observations is achieved by phenomenologically considering voltage-dependent relaxations of the electrode geometry.

2. Experiment

Distance-dependent force measurements were performed with a combined STM-AFM operated in ultrahigh vacuum (10^{-9} Pa) and at low temperature (5.5 K). PtIr tips attached to the free prong of a quartz tuning fork, which is referred to as the *qPlus* configuration [40], with resonance frequency ≈29 kHz and quality factor ≈55 000 served as force probes. For measuring the tunnelling current a separate wire is connected to the tip, similar to previous assemblies [1, 41–43]. Simultaneous distance-dependent current and force data were acquired using a low gain (10^4—10^6 V A^{-1}) of the transimpedance amplifier. The entailed bandwidths of 500–200 kHz exceed the resonance frequency of the tuning fork and its higher harmonics. This setup and operation mode ensure the absence of cross-talk between the tunnelling current and the AFM signal [43].

Prior to the experiments the AFM tip had been prepared *ex situ* by focused ion beam milling to ensure a well defined macroscopic shape of the apex. *In situ*, the tips were prepared by field emission on and indentation into the substrate surfaces, which presumably led to coating of the tip with substrate material and microscopic changes of the tip apex. The tips were further prepared by the transfer of a single tip apex atom to the surface [10, 11, 16, 19, 20]. Such tips are particularly stable, give rise to submolecular contrast in STM images of C_{60} and reliably show the signature of the Cu(111) Shockley surface state and the Bardeen–Cooper–Schrieffer energy gap of Pb(111) in spectra of the differential conductance (dI/dV). Due to this *in situ* preparation protocol the tips are likely terminated by a pyramidal cluster, as previously demonstrated by calculations for Cu(111) [10] and Pb(111) [16]. Termination of the tip apex with a single C_{60} molecule was routinely achieved by applying previously reported procedures [30, 44]. The orientation of the tip apex molecule was determined by imaging atomic protrusions on the surface [30, 45, 46].

Cu(111) and Pb(111) surfaces were prepared by Ar^+ bombardment and annealing. C_{60} molecules (purity: 99.95%) were sublimated from a heated Ta crucible onto the surfaces at room temperature. Ordered C_{60} superstructures on Cu(111) were obtained after annealing the C_{60}-covered surface at 400–500 K.

The vertical force, F, was calculated from the measured resonance frequency variation, Δf, using different deconvolution methods [47, 48], which led to virtually identical results. Distance $z = 0$ pm in force spectroscopy experiments is defined as the z position of the vertical force minimum at bias voltage $V = 0$ V. Tunnelling (Contact) ranges span distances $z < 0$ pm ($z > 0$ pm). STM images of the sample surfaces were recorded in the constant-current mode with V applied to the sample and processed using WSXM [49]. Spectra of dI/dV were acquired by modulating the dc bias voltage with an ac signal (10 mV (root-mean-square), 500 Hz) and measuring the first harmonic of the current response with a lock-in amplifier.

3. Results and discussion

In previous AFM experiments the tip–sample distance was varied and the resonance frequency change of the oscillating tuning fork simultaneously measured at a fixed bias voltage for various systems [44, 50–55]. The resulting force variation is of the Lennard–Jones (LJ) type that reflects the superposition of long-range van der Waals and electrostatic attraction and short-range Pauli repulsion. In particular, the force minimum signals the onset to chemical contact [44]. Additional forces have to be considered in the presence of magnetic materials [36, 56], ionic crystals or polar molecules [57, 58], and semiconducting surfaces [59].

The present experiments are in part motivated by a previous report on the voltage tuning of vibrational mode energies in single-molecule junctions [60]. A voltage-dependent shift of C_{60} vibrational energies was observed in simultaneous transport and surface-enhanced Raman spectroscopy experiments and rationalized in terms of a bias-driven charging of the molecule [60]. Concomitantly with the charging intramolecular as well as molecule–electrode chemical bonds are modified, which has direct impact on bond strengths and, thus, on forces that are required to induce structural relaxations. Therefore, force spectroscopy has been applied here to C_{60} junctions for a wide range of negative and positive bias voltages.

Figure 1 presents an illustration of the STM-AFM junction used in the experiments. A C_{60} molecule terminates a pyramidal tip apex and contacts a C_{60} molecule adsorbed on the substrate surface. The distances introduced in figure 1 will be explained in the following.

Figure 2 summarizes representative results obtained for a junction comprising a C_{60}-terminated PtIr tip and C_{60} adsorbed on a Cu(111) surface (figure 2(a)). In total, ten different tips were used for force measurements on ten C_{60} molecules for each individual tip. STM images of C_{60}-covered Cu(111) acquired with a C_{60}-terminated tip show a hexagonal arrangement of the molecules in single-layer islands (figure 2(b)). The trefoil-like submolecular pattern indicates a specific C_{60} orientation, where a C hexagon is exposed to the vacuum. In accordance with previous observations [61] and calculations [62, 63] these patterns are due to the next-to-lowest unoccupied molecular orbital. In addition, the STM data of figure 2(b) are compatible with a C_{60} orientation at the tip apex that exposes a C hexagon to the sample surface [63]. The inset to figure 2(b) shows an STM image of

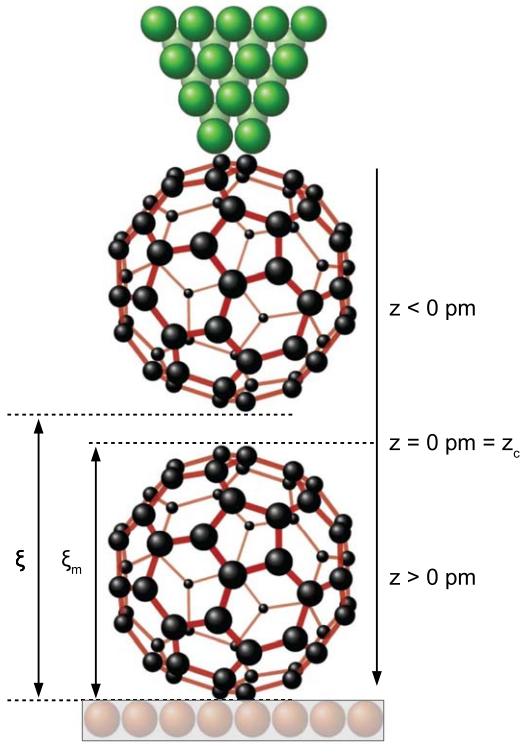

Figure 1. Sketch of a C_{60}–C_{60} junction with definition of distances. Distance $z = 0$ pm is defined as the point of maximum C_{60}–C_{60} attraction and referred to as z_c. Intervals $z < 0$ pm and $z > 0$ pm define, respectively, tunnelling and contact ranges. For estimating van der Waals forces the C_{60}-terminated tip is approximated as a metal sphere a distance ξ apart from a metal continuum (grey shaded area). Distance ξ_m denotes the distance between point-like particles in the Lennard–Jones potential (see text).

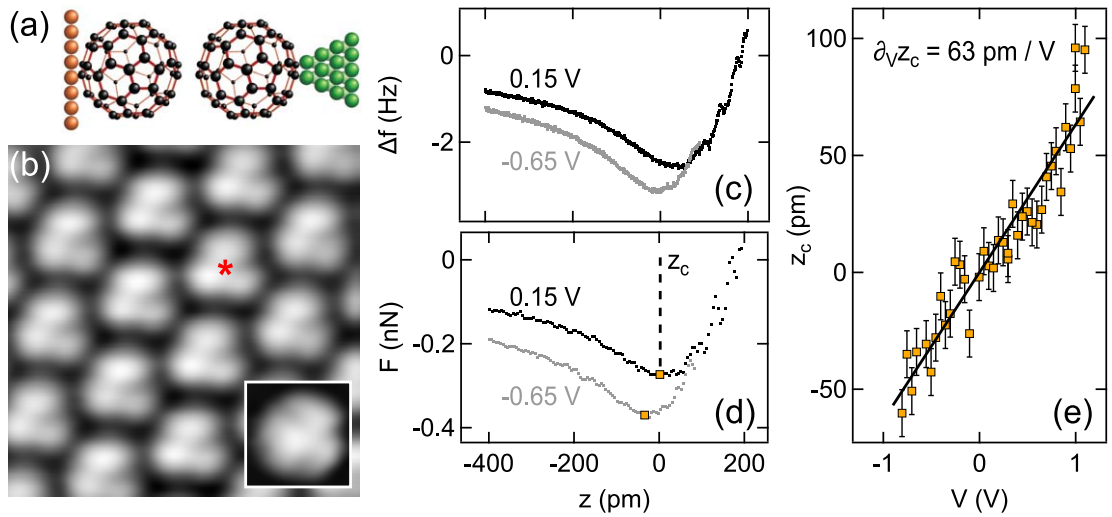

Figure 2. STM and AFM data for a junction comprising a C_{60}-terminated PtIr tip and a single C_{60} molecule on Cu(111). (a) Sketch of the junction configuration. (b) STM image of C_{60}-covered Cu(111) acquired with a C_{60}-terminated tip (1.5 V, 0.1 nA, 4.1×4.1 nm^2). The grey scale ranges from 0 pm (black) to 100 pm (white). Individual C_{60} molecules appear with a trefoil-like submolecular pattern. The asterisk indicates the center of a C_{60} molecule above which $\Delta f(z)$ data were recorded. Inset: STM image of a C_{60}-terminated tip using an atomic protrusion on Cu(111) (-2 V, 50 pA, 2.2×2.2 nm^2). The same grey scale as in (b) is used. (c) Δf as a function of z at the indicated bias voltages. The lower data set is vertically offset by -1 Hz. The feedback loop had been disabled at 1.5 V, 0.1 nA prior to data acquisition. (d) F calculated from the data shown in (c). The lower data set is vertically offset by -0.1 nN. Minima of F occur at z_c and are indicated by squares. (e) z_c as a function of V with indicated slope ($\partial_V z_c$) of the linear fit (solid line) to the data. The error bars for z_c result from the uncertainty in determining the force minimum using voltage-dependent force data.

the tip apex that was obtained by scanning the C_{60}-terminated tip across an atomic protrusion on Cu(111). The trefoil-like structural motif corroborates the C_{60} hexagon orientation at the tip apex.

$\Delta f(z)$ data (distance z is defined in figure 1) were recorded for C_{60} molecules embedded in an island. To this end, after positioning the tip atop the center of an adsorbed C_{60} molecule (asterisk in figure 2(b)) the feedback loop was disabled at the same current and sample voltage for all spectra, followed by the retraction of the tip to the same initial position and ramping the bias voltage to the desired value. $\Delta f(z)$ in tunnelling and contact ranges was then acquired by applying a linear voltage ramp to the z piezoceramic actuator hosting the probe. Figure 2(c) shows a representative evolution of Δf for the indicated bias voltages. Surprisingly, the minimum of Δf depends on the bias voltage.

The resulting vertical force (figure 2(d)) resembles the evolution of LJ-type forces, which is in accordance with previous experimental reports [44, 55]. The force trace exhibits a minimum at z_c, which signals the onset to molecule–molecule contact. Obviously, z_c depends on the bias voltage, which reflects the observed shift for Δf. The force at contact, $F_c \approx -280$ pN at 0.15 V, is in agreement with findings reported previously for C_{60}–C_{60} contacts on Cu(111) [44].

To explore the bias voltage dependence of the minimum of F, z_c is plotted for bias voltages ranging from -0.8 to 1.1 V in figure 2(e). The scattering of the data in figure 2(e) may be attributed to the uncertainty of the lateral tip position above C_{60}, which was previously estimated as ≈10% of the C_{60} diameter [44]. A systematic analysis of a possible dependence of $z_c(V)$ on the lateral tip position atop C_{60} was not performed in this study. More remarkably, an essentially linear increase of z_c from ≈ -60 pm at -0.8 V to ≈95 pm at 1.1 V is observed giving rise to a slope of $\partial_V z_c \approx 63$ pm V^{-1}. A weak quadratic component of $z_c(V)$ may be due to electrostatic forces (*vide infra*). Since the $z_c(V)$ behaviour is dominated by the linear term, the linear variation shall be elucidated in the following. Figure 2(e) shows that the onset to contact is shifted by more than 150 pm towards larger z_c. As will be discussed below, this shift does not reflect deformations of the C_{60} cage since it exhibits a high mechanical stiffness [64]. Rather, relaxations of the tip–C_{60} and C_{60}–substrate distances are more likely. For different microtips that were obtained by *in situ* tip preparation $\partial_V z_c$ varied between 60 and 95 pm V^{-1}. Some tips gave rise to negligible z_c shifts, i.e. $\partial_V z_c \approx 0$, which will be discussed at the end of the article.

It was further noticed that C_{60} molecules that are differently hybridized with Cu(111) behaved similarly in force spectroscopy experiments. The different C_{60} species are due to the coexistence of unreconstructed and reconstructed surface regions, which occur in the course of annealing the C_{60}-covered surface [65]. In reconstructed regions, 7 Cu atoms are removed below each adsorbed C_{60} molecule [65], which gives rise to a partial embedding of C_{60} into the substrate surface and an enhanced coordination with Cu atoms compared to C_{60} on unreconstructed Cu(111).

In order to explore whether the findings reported for C_{60}–C_{60} junctions (figure 2) are of general character, additional experiments were performed with clean PtIr tips and C_{60} adsorbed on Pb(111) (figure 3(a)), i.e. for markedly different junctions. C_{60} molecules on Pb(111) arrange in a hexagonal array, as depicted in the STM image in figure 3(b). In addition to the molecular superstructure a moiré pattern is visible as the periodic modulation of the apparent height of C_{60} molecules. For clarity the unit cell of the moiré lattice is indicated by the dashed lozenge. The moiré periodicity, 4.55 ± 0.24 nm, is in agreement with one of the previously reported higher-order commensurate structures [66].

Bias-dependent force measurements were performed on individual C_{60} molecules residing inside molecular islands, analogously to the aforementioned experiments for C_{60} on Cu(111). The same number of tips and molecules were explored as in the case of Cu(111). Figures 3(c) and (d) depict the resulting evolution of, respectively, Δf and F. Again, the minima of Δf and, thus, F depend on the bias voltage. The minimum z_c exhibits an essentially linear increase with the bias voltage (figure 3(e)), gradually shifting from ≈ -53 pm at -1.4 V to ≈60 pm at 1.2 V. The linear fit (solid line in figure 3(e)) to the data exhibits a slope of $\partial_V z_c \approx 43$ pm V^{-1}. Therefore, the onset to contact is shifted by more than 100 pm towards the molecule in the probed V range, which is in accordance with the findings for C_{60}–C_{60} junctions (figure 2).

The monotonic shift of z_c with V is remarkable since, as will be demonstrated next, it is not described by the superposition of long-range van der Waals and electrostatic together with short-range Pauli forces using conventional expressions for these forces. To see this, long-range and slowly varying van der Waals forces, F_{vdW}, were derived from the interaction energy $E_{vdW} = -HR/(6\xi)$ (H: Hamaker constant) [67] between a metallic sphere of radius R and a semi-infinite metal, a distance ξ from the sphere (figure 1). In addition, the attractive part of the LJ interaction energy, $E_{LJ} = \varepsilon[(\xi_m/\xi)^{12} - 2 \cdot (\xi_m/\xi)^6]$ (ε: depth of the LJ potential well), contributes to the van der Waals forces. The LJ interaction energy likewise contains the short-range repulsive part that is responsible for the Pauli force. E_{LJ} considers the interaction of two point-like particles with equilibrium distance ξ_m (figure 1). The point-like particle representing the C_{60} molecule was positioned 0.7 nm above the metal surface, which corresponds to the molecular diameter. The electrostatic force, F_{el}, between a spherical tip and a semi-infinite planar sample was inferred from the energy $E_{el} = \pi\varepsilon_0 R(V - V_{cp})^2 \ln\xi$ (ε_0: vacuum permittivity, V_{cp}: contact voltage) [68]. V_{cp} was extracted from the bias voltage evolution of the vertical

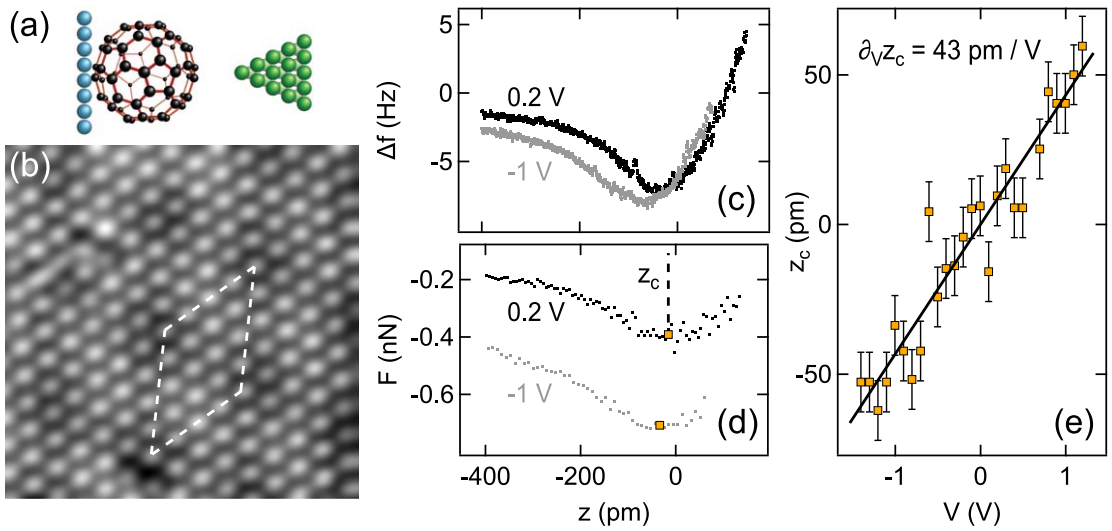

Figure 3. STM and AFM data for a junction comprising a PtIr tip and a single C_{60} molecule on Pb(111). (a) Sketch of the junction configuration. (b) STM image of C_{60}-covered Pb(111) (30 mV, 10 pA, 13 × 13 nm^2). The grey scale ranges from 0 pm (black) to 100 pm (white). Individual molecules appear as circular protrusions that are arranged in a hexagonal lattice. The apparent height of C_{60} molecules is modulated due to a moiré superstructure whose unit cell is indicated as a dashed line. (c) Resonance frequency variation, Δf, as a function of piezo displacement, z, for the indicated bias voltages. The lower data set is vertically offset by −4 Hz. The feedback loop had been disabled at 1.5 V, 12 pA prior to data acquisition. (d) Vertical force, F, calculated from the data shown in (c). The lower data set is vertically offset by −0.1 nN. Minima of F occur at z_c and are indicated by squares. (e) z_c as a function of V. The slope ($\partial_V z_c$) of the linear fit (solid line) is indicated. The error bars for z_c result from the uncertainty in determining the force minimum using voltage-dependent force data.

force, $F(V)$ (not shown). In order to facilitate comparison with experimental data, a piezo displacement z is calculated from the electrode separation ξ via $z = \xi_{c,0} - \xi$ with $\xi_{c,0}$ the distance at maximum attraction for $V = 0$ V.

The C_{60}–C_{60} interaction was modelled by the LJ potential owing to its significantly better agreement with experimental data than obtained for the Girifalco potential [69]. Indeed, using the Girifalco potential that was originally conceived for the interaction between two free C_{60} molecules gives rise to considerable deviations from experimental data. Most likely, the C_{60}–tip and C_{60}–surface hybridization and concomitant charge transfer render the Girifalco potential a less appropriate description of the metallic C_{60}–C_{60} contact presented here. A better agreement between force data and the Girifalco picture was previously reported for C_{60}-terminated tips and C_{60} adsorbed on Si(111) [70], which hints at the nearly free-molecule character on a semiconductor surface. Moreover, $z_c(V)$ is similar for C_{60}-terminated tips (figure 2(e)) and metal tips (figure 3(e)) that are presumably terminated by a single atom, which corroborates the deviation of C_{60} adsorbed to the metal tip from its free-molecule state and further justifies the use of the LJ potential.

The modelling of the C_{60} molecule as a metallic sphere in the expression of van der Waals and electrostatic interactions certainly represents an approximation. The metallic or dielectric nature of a C_{60} molecule was debated in several works with contradictory conclusions [71–73]. In the present case, the metal-sphere approximation is appropriate since $F(V)$ recorded for a wide range of tip-surface distances covering tunnelling to contact exhibits parabolic behaviour, which is expected for the electrostatic force between a metal sphere and a semi-infinite metal. The similar behaviour of $z_c(V)$ for C_{60}-terminated tips and metal PtIr tips (*vide supra*) further supports the metallic character of the C_{60} tip.

Forces due to permanent and induced molecular dipoles were not considered since their contribution to the total force F is negligible. In simulations based on density functional theory (not shown), C_{60} was adsorbed with a C hexagon on a 4-layer Cu(111) slab modelling the substrate and on a triangular Cu cluster adsorbed to a 4-layer Cu(111) slab serving as a tip. Permanent dipoles due to charge transfer processes were calculated as ≈1.5 D (1 D = 1 Debye = $3.3356 \cdot 10^{-30}$ Cm) for C_{60} adsorbed on Cu(111) and ≈1.8 D for C_{60} on the tip at a distance between the facing C hexagons of 0.6 nm. Near contact, i.e. at a mutual C hexagon distance of 0.25 nm, the dipoles decreased to ≈1.2 D for C_{60} on Cu(111) and to ≈1.3 D for C_{60} on the tip due to reorganization of the accumulated charge at chemical-bond distances. Considering the molecules as point dipoles at distances 0.6 nm and 0.25 nm led to dipole–dipole forces of, respectively, $4 \cdot 10^{-3}$ nN and $3 \cdot 10^{-3}$ nN, which are two orders of magnitude lower than the measured total force. The induced dipole at 1 V may be estimated by using the experimentally determined polarizability of isolated C_{60} (0.076 5 nm^3) [74], which yields an electric dipole moment of ≈0.2 D being even lower than the permanent dipole. Dipole moments of metal tips, which are

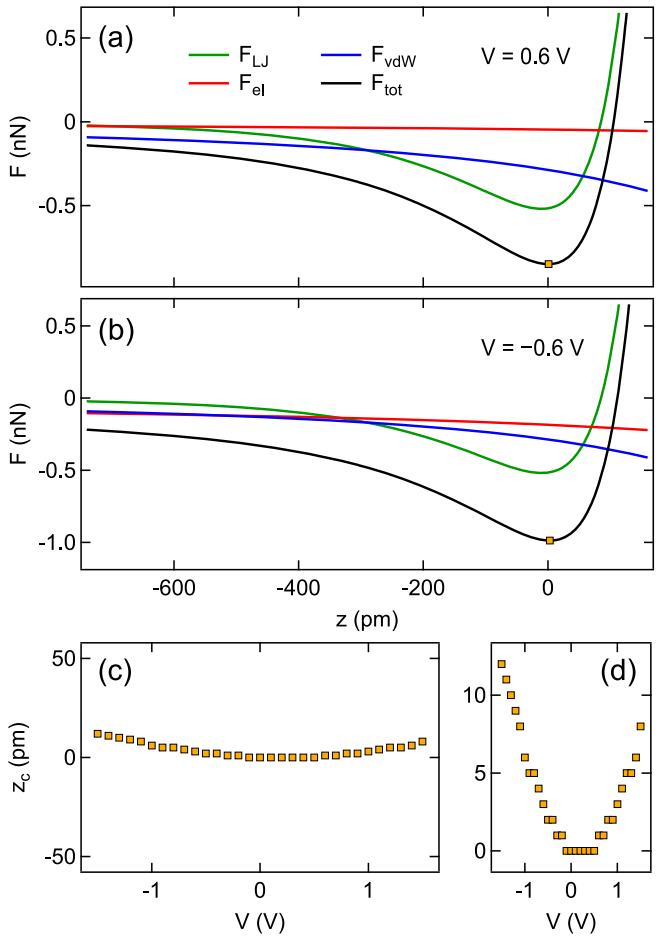

Figure 4. Calculated F_{LJ}, F_{el}, F_{vdW}, F_{tot} for (a) 0.6 V and (b) −0.6 V assuming a rigid junction geometry. Parameters entering into the underlying interaction energies are based on experimental values: $V_{cp} = 0.2$ V, $\xi_m = 0.9$ nm and $\varepsilon = 1.1$ eV, $R = 10$ nm [77], $H = 1$ eV [78] (see text for the analytical expressions of interaction energies). The squares indicate minima of F_{tot} at z_c. (c) z_c as a function of V. (d) Close-up view of (c) showing the parabolic response of $z_c(V)$ to electrostatic forces.

Table 1. Parameters and references used for the force simulations shown in figures 4 and 5.

	R (nm)	ξ_m (nm)	H (eV)	ε (eV)	V_{cp} (V)	α (pm V^{-1})
	10	0.9	1.0	1.1	0.2	30
Reference	[77]	This work	[78]	This work	This work	This work

relevant to the PtIr–C_{60} contacts, were previously demonstrated to be on the order of several Debyes below 10 D [75, 76]. Therefore, resulting dipole–dipole forces are still much smaller than the total force.

The superposition, $F_{tot} = F_{vdW} + F_{el} + F_{LJ}$, is plotted as a function of z in figure 4(a) for 0.6 V and in figure 4(b) for −0.6 V. F_{tot} was calculated for bias voltages between −1.5 and 1.5 V leading to the z_c evolution presented in figure 4(c). Table 1 summarizes the parameters used for the simulations in figures 4 and 5. z_c depends weakly and in a non-monotonic way on V deviating from the experimentally observed evolution (figures 2(e), 3(e)). The close-up view of $z_c(V)$ in figure 4(d) shows a parabola-like behaviour with a minimum at ≈0.2 V, which reflects the response to the electrostatic force that is proportional to $(V - V_{cp})^2$ with measured $V_{cp} \approx 0.2$ V. Consequently, the superposition $F_{vdW} + F_{el} + F_{LJ}$ using conventional expressions for the individual forces fails in describing bias-dependent force data.

In identifying possible origins for the observed bias voltage dependence of z_c several scenarios were excluded. First, C_{60} is a non-polar molecule with a high polarizability [74, 79]. Therefore, the electric field across the C_{60}–C_{60} junction polarizes the molecules giving rise to induced dipole moments. However, dipole–dipole forces are negligible in the present setup (*vide supra*). Second, variations in $\Delta f(z)$ may be induced by high sample resistances on the order of 100 MΩ [59]. For the presented C_{60}–C_{60} (PtIr–C_{60}) contacts a resistance of ≈600 kΩ (≈60 kΩ) was measured, which is nearly 3 (4) orders of magnitude lower than the resistances relevant to appreciable Δf [59]. Therefore, this scenario is excluded as well. Third, electron wind forces that are due to

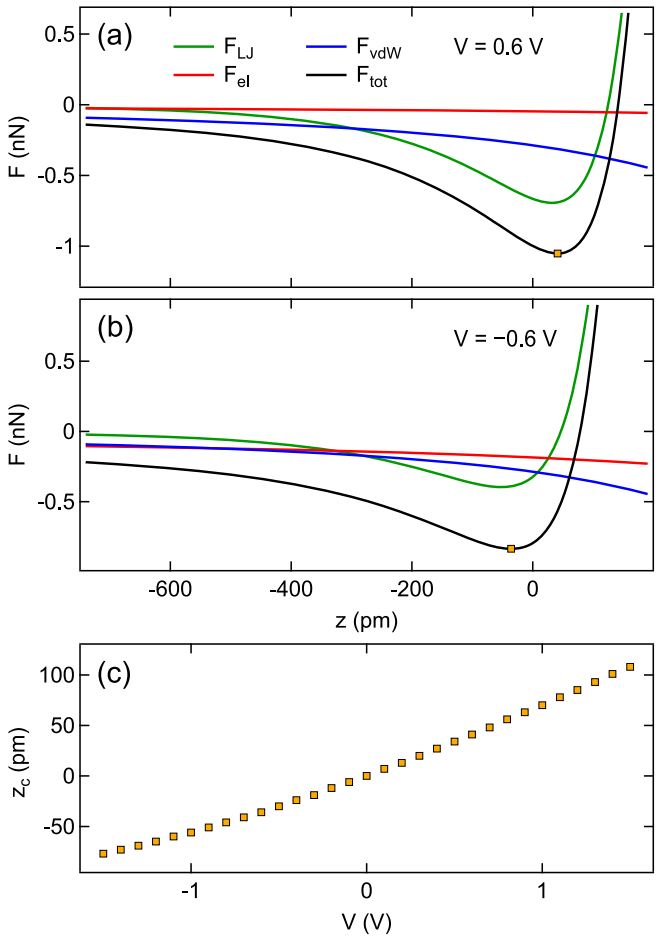

Figure 5. Like figure 4, considering voltage-dependent relaxations of the junction geometry in F_{LJ} by $\xi + \alpha V$ ($\alpha = 30$ pm V^{-1}).

momentum transfer from transported electrons to ions [80] exhibit a complex energy dependence, as previously demonstrated by calculations for a single-molecule junction [81]. The linear shift of z_c with V is not compatible with this complicated energy dependence and, hence, cannot be rationalized in terms of electron wind.

In the following, junction relaxations depending on the bias voltage are considered. To this end, a bias-dependent electrode separation, $\xi + \alpha V$, is phenomenologically included in the LJ interaction energy. This suggestion is motivated by a previous density functional theory (DFT) study that revealed new equilibrium positions and orientations of C_{60} in an external electric field [82]. DFT also demonstrated the linear dependence of the distance between a negatively charged oxygen atom and the supporting graphene sheet on the external electric field [83]. In addition, it was shown on theoretical grounds that a current flowing across nanometre-sized objects induces the non-equilibrium population of electronic states with a concomitant weakening of intramolecular bonds that leads to a deformation of the molecular object [60, 84, 85].

Figure 5 summarizes the calculated results considering voltage-dependent relaxations in F_{LJ}. In contrast to the assumption of a rigid junction geometry (figure 4) the position of the force minimum, z_c (squares in figures 5(a), (b)), varies considerably with the bias voltage (figure 5(c)). Using $\alpha = 30$ pm V^{-1} leads to a monotonic evolution of z_c with V (figure 5(c)) in a distance range comparable with the experimental observations (figures 2(e), 3(e)). A linear component with slope ≈63 pm V^{-1} dominates the monotonic increase of z_c with V.

The suggested bias-dependent relaxations may intuitively be understood by considering charge transfer processes. It was previously shown that adsorption of C_{60} on Cu and Pb surfaces leads to electron transfer from the substrate to the molecule [65, 86–89]. Therefore, in PtIr–C_{60} junctions the negatively charged C_{60} adsorbed on Pb(111) is attracted to (repelled from) the positively (negatively) charged sample at positive (negative) bias voltage. This simple picture is consistent with the bias voltage evolution of z_c in these junctions.

In the case of C_{60}-terminated tips the aforementioned picture does not directly hold, in the following sense. Assuming similarly charged C_{60} molecules at the tip and on the surface as well as taking into account smaller tip–C_{60} than C_{60}–substrate interactions [44] would lead to similar z_c at negative and positive bias voltage, which is not in agreement with the observation (figure 2(e)). Therefore, the assumption of similarly charged C_{60}

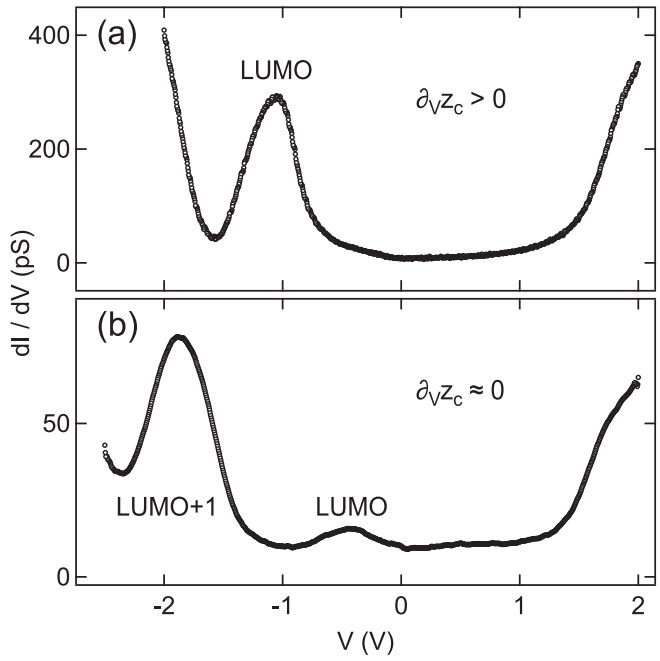

Figure 6. Spectra of dI/dV acquired atop clean Cu(111) with C_{60}-terminated tips exhibiting a (a) large and (b) small z_c shift with the bias voltage. Signatures of the C_{60} lowest unoccupied molecular orbital (LUMO) and LUMO + 1 are visible at negative bias voltage. Feedback loop parameters: (a) 2 V, 500 pA; (b) 2 V, 40 pA.

molecules may not be applicable. The comparison of dI/dV spectra of C_{60}-terminated tips with non-zero ($\partial_V z_c > 0$, figure 6(a)) and negligible ($\partial_V z_c \approx 0$, figure 6(b)) z_c variations helps clarify this issue. Spectroscopic features appearing at negative bias voltage correspond to unoccupied states of C_{60} at the tip. In particular, the lowest unoccupied molecular orbital (LUMO) is more than 1 eV below the Fermi energy (E_F, $V = 0$ V) for C_{60}-terminated tips with $\partial_V z_c > 0$ (figure 6(a)). In contrast, C_{60}-terminated tips with the LUMO spectroscopic signature much closer to E_F (figure 6(b)) exhibit a weak shift ($\partial_V z_c \approx 0$) at most. The vicinity of the C_{60} LUMO to E_F is a measure for the extent of the charge transfer between the molecule and the metal substrate it is adsorbed on [90]. In particular, C_{60} tips with $\partial_V z_c > 0$ ($\partial_V z_c \approx 0$) represent C_{60} molecules that received a comparatively low (high) amount of charge from the metal tip. Therefore, C_{60} molecules at the tip with $\partial_V z_c > 0$ (figure 6(a)) are less susceptible to the electric field in the junctions and behave in a similar manner as observed for the clean PtIr tip. C_{60} molecules subject to larger charge transfer (figure 6(b)) exhibit a stronger displacement in the electric field and give rise to a reduced z_c shift. The larger charge transfer may be related to C_{60} adsorption at rather blunt tip regions, which involves more tip atoms than in the case of sharper tips.

4. Conclusions

The point of maximum attraction in single-molecule contacts has been explored by distance-dependent force measurements and is subject to the bias voltage across the junction. Structural relaxations of the electrode atomic geometry induced by the electric field between tip and sample acting on partially charged molecules can account for the experimental observations. The presented findings are relevant to chemical reactions in external fields at the single-molecule level.

Acknowledgements

Discussions with N Hauptmann (Nijmegen, The Netherlands), sharing data with S Leitherer and M Brandbyge (Lyngby, Denmark) prior to publication and funding by the Deutsche Forschungsgemeinschaft through Grant No. KR 2912/12-1 is acknowledged.

ORCID iDs

N Néel https://orcid.org/0000-0003-0498-9138
J Kröger https://orcid.org/0000-0002-6452-5864

References

[1] Gross L, Mohn F, Moll N, Liljeroth P and Meyer G 2009 *Science* **325** 1110–4
[2] de Oteyza D G *et al* 2013 *Science* **340** 1434–7
[3] Pavliček N and Gross L 2017 *Nat. Rev. Chem.* **1** 16014
[4] Ternes M, Lutz C P, Hirjibehedin C F, Giessibl F J and Heinrich A J 2008 *Science* **319** 1066–9
[5] Dürig U, Züger O and Pohl D W 1990 *Phys. Rev. Lett.* **65** 349–52
[6] Olesen L, Brandbyge M, Sørensen M R, Jacobsen K W, Lægsgaard E, Stensgaard I and Besenbacher F 1996 *Phys. Rev. Lett.* **76** 1485–8
[7] Cross G, Schirmeisen A, Stalder A, Grütter P, Tschudy M and Dürig U 1998 *Phys. Rev. Lett.* **80** 4685–8
[8] Hofer W A, Fisher A J, Wolkow R A and Grütter P 2001 *Phys. Rev. Lett.* **87** 236104
[9] Rubio-Bollinger G, Joyez P and Agraït N 2004 *Phys. Rev. Lett.* **93** 116803
[10] Limot L, Kröger J, Berndt R, Garcia-Lekue A and Hofer W A 2005 *Phys. Rev. Lett.* **94** 126102
[11] Kröger J, Jensen H and Berndt R 2007 *New J. Phys.* **9** 153
[12] Kröger J, Néel N, Sperl A, Wang Y F and Berndt R 2009 *New J. Phys.* **11** 125006
[13] Calvo M R, Sabater C, Dednam W, Lombardi E B, Caturla M J and Untiedt C 2018 *Phys. Rev. Lett.* **120** 076802
[14] Sabater C, Dednam W, Calvo M R, Fernández M A, Untiedt C and Caturla M J 2018 *Phys. Rev.* B **97** 075418
[15] Trouwborst M L, Huisman E H, Bakker F L, van der Molen S J and van Wees B J 2008 *Phys. Rev. Lett.* **100** 175502
[16] Müller M, Salgado C, Néel N, Palacios J J and Kröger J 2016 *Phys. Rev.* B **93** 235402
[17] Hölscher H, Schirmeisen A and Schwarz U D 2008 *Phil. Trans. R. Soc.* A **366** 1383–404
[18] Agraït N, Yeyati A L and van Ruitenbeek J M 2003 *Phys. Rep.* **377** 81–279
[19] Kröger J, Néel N and Limot L 2008 *J. Phys.: Condens. Matter* **20** 223001
[20] Berndt R, Kröger J, Néel N and Schull G 2010 *Phys. Chem. Chem. Phys.* **12** 1022–32
[21] Scheer E, Agraït N, Cuevas J C, Yeyati A L, Ludoph B, Martín-Rodero A, Bollinger G R, van Ruitenbeek J M and Urbina C 1998 *Nature* **394** 154–7
[22] Hiraoka R, Arafune R, Tsukahara N, Kawai M and Takagi N 2014 *Phys. Rev.* B **90** 241405
[23] Néel N, Kröger J, Limot L and Berndt R 2008 *Nano Lett.* **8** 1291–5
[24] Wang Y, Kröger J, Berndt R and Hofer W A 2009 *J. Am. Chem. Soc.* **131** 3639–43
[25] Lafferentz L, Ample F, Yu H, Hecht S, Joachim C and Grill L 2009 *Science* **323** 1193–7
[26] Néel N, Kröger J and Berndt R 2011 *Nano Lett.* **11** 3593–6
[27] Auwärter W, Seufert K, Bischoff F, Ecija D, Vijayaraghavan S, Joshi S, Klappenberger F, Samudrala N and Barth J V 2012 *Nat. Nanotechnol.* **7** 41–6
[28] Brand J, Ribeiro P, Néel N, Kirchner S and Kröger J 2017 *Phys. Rev. Lett.* **118** 107001
[29] Wang Y F, Kröger J, Berndt R, Vázquez H, Brandbyge M and Paulsson M 2010 *Phys. Rev. Lett.* **104** 176802
[30] Schull G, Frederiksen T, Arnau A, Sanchez-Portal D and Berndt R 2011 *Nat. Nanotechnol.* **6** 23–7
[31] Yamada T K, Bischoff M M J, Mizoguchi T and van Kempen H 2003 *Appl. Phys. Lett.* **82** 1437–9
[32] Berbil-Bautista L, Krause S, Bode M and Wiesendanger R 2007 *Phys. Rev.* B **76** 064411
[33] Néel N, Kröger J and Berndt R 2009 *Phys. Rev. Lett.* **102** 086805
[34] Rodary G, Wedekind S, Oka H, Sander D and Kirschner J 2009 *Appl. Phys. Lett.* **95** 152513
[35] Ziegler M, Ruppelt N, Néel N, Kröger J and Berndt R 2010 *Appl. Phys. Lett.* **96** 132505
[36] Lazo C, Néel N, Kröger J, Berndt R and Heinze S 2012 *Phys. Rev.* B **86** 180406
[37] Schöneberg J, Otte F, Néel N, Weismann A, Mokrousov Y, Kröger J, Berndt R and Heinze S 2016 *Nano Lett.* **16** 1450–4
[38] Schmaus S, Bagrets A, Nahas Y, Yamada T K, Bork A, Bowen M, Beaurepaire E, Evers F and Wulfhekel W 2011 *Nat. Nanotechnol.* **6** 185–9
[39] Ziegler M, Néel N, Lazo C, Ferriani P, Heinze S, Kröger J and Berndt R 2011 *New J. Phys.* **13** 085011
[40] Giessibl F J 1998 *Appl. Phys. Lett.* **73** 3956–8
[41] Heyde M, Sterrer M, Rust H P and Freund H J 2005 *Appl. Phys. Lett.* **87** 083104
[42] Albers B J, Liebmann M, Schwendemann T C, Baykara M Z, Heyde M, Salmeron M, Altman E I and Schwarz U D 2008 *Rev. Sci. Instrum.* **79** 033704
[43] Majzik Z, Setvín M, Bettac A, Feltz A, Cháb V and Jelínek P 2012 *Beilstein J. Nanotechnol.* **3** 249–59
[44] Hauptmann N, Mohn F, Gross L, Meyer G, Frederiksen T and Berndt R 2012 *New J. Phys.* **14** 073032
[45] Kelly K F, Sarkar D, Prato S, Resh J S, Hale G D and Halas N J 1996 *J. Vac. Sci. Technol.* B **14** 593–6
[46] Schull G, Frederiksen T, Brandbyge M and Berndt R 2009 *Phys. Rev. Lett.* **103** 206803
[47] Sader J E and Jarvis S P 2004 *Appl. Phys. Lett.* **84** 1801–3
[48] Giessibl F J 2001 *Appl. Phys. Lett.* **78** 123–5
[49] Horcas I, Fernández R, Gómez-Rodríguez J M, Colchero J, Gómez-Herrero J and Baro A M 2007 *Rev. Sci. Instrum.* **78** 013705
[50] Lantz M, O'Shea S and Welland M 1999 *Surf. Sci.* **437** 99– 106
[51] Schirmeisen A, Cross G, Stalder A, Grütter P and Dürig U 2000 *New J. Phys.* **2** 29
[52] Sun Y, Mortensen H, Schär S, Lucier A S, Miyahara Y, Grütter P and Hofer W 2005 *Phys. Rev.* B **71** 193407
[53] Sawada D, Sugimoto Y, Morita K I, Abe M and Morita S 2009 *Appl. Phys. Lett.* **94** 173117
[54] Ternes M, González C, Lutz C P, Hapala P, Giessibl F J, Jelínek P and Heinrich A J 2011 *Phys. Rev. Lett.* **106** 016802
[55] Pawlak R, Kawai S, Fremy S, Glatzel T and Meyer E 2011 *ACS Nano* **5** 6349–54
[56] Kaiser U, Schwarz A and Wiesendanger R 2007 *Nature* **446** 522–5
[57] Schneiderbauer M, Emmrich M, Weymouth A J and Giessibl F J 2014 *Phys. Rev. Lett.* **112** 166102
[58] Corso M, Ondráček M, Lotze C, Hapala P, Franke K J, Jelínek P and Pascual J I 2015 *Phys. Rev. Lett.* **115** 136101
[59] Weymouth A J, Wutscher T, Welker J, Hofmann T and Giessibl F J 2011 *Phys. Rev. Lett.* **106** 226801
[60] Li Y, Doak P, Kronik L, Neaton J B and Natelson D 2014 *Proc. Natl Acad. Sci.* **111** 1282–7
[61] Abel M, Dmitriev A, Fasel R, Lin N, Barth J V and Kern K 2003 *Phys. Rev.* B **67** 245407
[62] Hands I D, Dunn J L and Bates C A 2010 *Phys. Rev.* B **81** 205440
[63] Lakin A J, Chiutu C, Sweetman A M, Moriarty P and Dunn J L 2013 *Phys. Rev.* B **88** 035447
[64] Néel N, Kröger J, Limot L, Frederiksen T, Brandbyge M and Berndt R 2007 *Phys. Rev. Lett.* **98** 065502
[65] Pai W W *et al* 2010 *Phys. Rev. Lett.* **104** 036103
[66] Li H I, Franke K J, Pascual J I, Bruch L W and Diehl R D 2009 *Phys. Rev.* B **80** 085415
[67] Hamaker H 1937 *Physica* **4** 1058–72

[68] Hudlet S, Saint Jean M, Guthmann C and Berger J 1998 *Eur. Phys. J.* B **2** 5–10
[69] Girifalco L A 1991 *J. Phys. Chem.* **95** 5370–1
[70] Chiutu C, Sweetman A M, Lakin A J, Stannard A, Jarvis S, Kantorovich L, Dunn J L and Moriarty P 2012 *Phys. Rev. Lett.* **108** 268302
[71] Stace A J and Bichoutskaia E 2011 *Phys. Chem. Chem. Phys.* **13** 18339–46
[72] Zettergren H and Cederquist H 2012 *Phys. Chem. Chem. Phys.* **14** 16770
[73] Raggi G, Stace A J and Bichoutskaia E 2013 *Phys. Chem. Chem. Phys.* **15** 20115–9
[74] Antoine R, Dugourd P, Rayane D, Benichou E, Broyer M, Chandezon F and Guet C 1999 *J. Chem. Phys.* **110** 9771–2
[75] Teobaldi G, Lämmle K, Trevethan T, Watkins M, Schwarz A, Wiesendanger R and Shluger A L 2011 *Phys. Rev. Lett.* **106** 216102
[76] Gao D Z, Grenz J, Watkins M B, Federici Canova F, Schwarz A, Wiesendanger R and Shluger A L 2014 *ACS Nano* **8** 5339–51
[77] Vasile M J, Grigg D A, Griffith J E, Fitzgerald E A and Russell P E 1991 *Rev. Sci. Instrum.* **62** 2167–71
[78] Hutter J L and Bechhoefer J 1993 *Rev. Sci. Instrum.* **64** 1868–73
[79] Ballard A, Bonin K and Louderback J 2000 *J. Chem. Phys.* **113** 5732–5
[80] Ventra M D 2008 *Electrical Transport in Nanoscale Systems* (Cambridge: Cambridge University Press)
[81] Hsu B C, Amanatidis I, Liu W L, Tseng A and Chen Y C 2014 *J. Phys. Chem.* C **118** 2245–52
[82] Stadler R, Kubatkin S and Bjørnholm T 2007 *Nanotechnology* **18** 165501
[83] Topsakal M, Gürel H H and Ciraci S 2013 *J. Phys. Chem.* C **117** 5943–52
[84] Di Ventra M, Pantelides S T and Lang N D 2002 *Phys. Rev. Lett.* **88** 046801
[85] Bai M, Cucinotta C S, Jiang Z, Wang H, Wang Y, Rungger I, Sanvito S and Hou S 2016 *Phys. Rev.* B **94** 035411
[86] Tsuei K D, Yuh J Y, Tzeng C T, Chu R Y, Chung S C and Tsang K L 1997 *Phys. Rev.* B **56** 15412–20
[87] Tzeng C T, Lo W S, Yuh J Y, Chu R Y and Tsuei K D 2000 *Phys. Rev.* B **61** 2263–72
[88] Larsson J A, Elliott S D, Greer J C, Repp J, Meyer G and Allenspach R 2008 *Phys. Rev.* B **77** 115434
[89] Schulze G, Franke K J and Pascual J I 2008 *New J. Phys.* **10** 065005
[90] Schull G, Néel N, Becker M, Kröger J and Berndt R 2008 *New J. Phys.* **10** 065012